GEOPHYSICS, VOL. 84, NO. 2 (MARCH-APRIL 2019); P. 1–15, 11 FIGS., 3 TABLES.
10.1190/GEO2018-0444.1

Case History

Structural complexity inferred from anisotropic resistivity: Example from airborne EM and compilation of historical resistivity/induced polarization data from the gold-rich Canadian Malartic district, Québec, Canada

Reza Mir[1], Stéphane Perrouty[1], Thibaut Astic[2], Charles L. Bérubé[3], and Richard S. Smith[1]

ABSTRACT

Structurally complex zones within orogenic terranes typically correspond to areas where there is interference between multiple fold generations and are known to be favorable pathways for fluid flow because of their higher permeability. In the Canadian Malartic district, gold anomalies have been linked with zones of structural complexity that have been quantified by outcrop bedding orientation measurements and calculation of bedding variance maps. In this work, historical apparent resistivity and induced polarization data in the Canadian Malartic district were reprocessed and combined with new surveys to create a compilation of inverted chargeability and resistivity, which were then interpreted together with airborne electromagnetics and outcrop structural data. The results indicate chargeability anomalies, up to five times the background value, associated with the sulfide mineral content in monzodioritic dikes that are thickened in folds and hydrothermally altered. Although the airborne apparent half-space resistivity is mostly sensitive to conductive surficial cover, the inverted ground resistivity method is sensitive to deeper structure and likely represents bedrock signal at depths greater than 25 m. Inverted ground resistivity exhibits strong anisotropy in areas of subvertical bedding, where measured resistivities can vary by up to a factor of two, over the same location, depending on whether the survey lines are perpendicular or parallel to the strike of bedding. This result is observed at scales of 50 cm up to 100 m. Analysis of inverted ground resistivity together with bedding variance indicates a strong correlation between structurally complex zones with high bedding variance and a decrease in resistivity at depths greater than 25 m. This suggests that in places where the presence of disseminated gold cannot be directly detected, or where the outcrop exposure is limited due to overburden cover, geophysical data may still succeed in identifying structural complexity zones that could potentially host mineralization.

INTRODUCTION

Orogenic gold deposits, such as those found in the Abitibi Greenstone Belt, are commonly controlled by major crustal breaks (e.g., the Cadillac Larder Lake Deformation Zone [CLLDZ], Dubé and Gosselin, 2007; Bedeaux et al., 2017), secondary fault zones, and/or by major fold hinges (Bierlein and Maher, 2001; Large et al., 2007; Perrouty et al., 2015; Groves et al., 2018). The identification of such structurally complex zones using geophysical data would be a major advantage for exploration projects in polydeformed terranes: in greenfields to outline the most prospective areas and in brownfields to locate ore shoots. The direct detection of mineralized areas by geophysical methods is highly challenging and, unfortunately, is rarely successful during exploration for disseminated gold deposits. Detection is further complicated by the presence of minerals that have a geophysical response but are not of economic interest, for

Manuscript received by the Editor 18 June 2018; revised manuscript received 25 October 2018; published ahead of production 18 December 2018.
[1]Laurentian University, Harquail School of Earth Sciences, 935 Ramsey Lake Road, Sudbury, Ontario P3E 2C6, Canada. E-mail: rmir@laurentian.ca; sperrouty@laurentian.ca; rssmith@laurentian.ca.
[2]University of British Columbia, Department of Earth, Ocean and Atmospheric Sciences, 2329 West Mall, Vancouver, British Columbia V6T 1Z4, Canada. E-mail: thast@eos.ubc.ca.
[3]Polytechnique Montréal, Département des Génies Civil, Géologique et des Mines, 2900 Edouard Montpetit Blvd, Montreal, Quebec H3T 1J4, Canada. E-mail: charles.lafreniere-berube@polymtl.ca.

example, disseminated barren sulfides that have a strong induced polarization (IP) response. Direct geophysical detection requires that the presence of a buried economic target significantly change the physical properties of the volume of interest in comparison to the background, so that there is a measurable contrast. This is a demanding requirement in the case of large disseminated gold deposits or where strong heterogeneities in the host rocks mask the subtle contrasts due to the deposit. Instead, we propose to use geophysical data to determine the spatial variation of structural complexity, which is a proxy for potential gold mineralization (Perrouty et al., 2017). The structural complexity of an area can usually be determined by outcrop observations (e.g., detailed structural mapping and structural measurements). However, in areas with poor or limited outcrop, due to overburden cover (e.g., glacial till in Canada) or intense weathering (e.g., laterite in Australia, Africa, and South America), this information will be difficult to obtain without resorting to drilling. In such cases, geophysical methods such as airborne magnetics, electromagnetics (EM), or ground resistivity/IP can be of great value in understanding the subsurface structure.

In this work, the area surrounding the Canadian Malartic deposit (estimated reserve of more than 18.6 Moz [578.46 tonnes] Au; Gervais et al., 2014) will be used as a case study to test an approach involving the integration of geophysical and structural data. The intrusion-related Canadian Malartic gold deposit is hosted within the metasedimentary rocks of the Pontiac Subprovince of the Archean Superior craton. This 280 km² area includes the Canadian Malartic world-class gold deposit (Derry, 1939; De Souza et al., 2016) and several gold occurrences with extensive alteration halos (Cartier, Gouldie, and Bravo, Figure 1). Previous work in the area highlighted a strong correlation between the presence of gold and the structurally complex zones, which can be outlined using the variance of bedding dips (Perrouty et al., 2017). These structurally complex areas were interpreted to represent multiple fold hinge interference domains, i.e., more permeable zones that acted as favorable pathways for fluid flow, hydrothermal alteration, and, locally, gold mineralization. At the Canadian Malartic deposit, the use of airborne magnetic data has been hampered by the presence of the strongly remanent magnetized, ultramafic rocks of the Piché group along the CLLDZ (Figure 1). The strong magnetic signal from these rocks masks the much weaker and relatively homogeneous magnetic signature of the adjacent Pontiac group (Bérubé et al., 2018). This raises the question, can airborne EM (AEM) and ground resistivity/IP be used to interpret structural complexity and locate potentially mineralized zones? These methods provide continuous data sets as opposed to measurement of bedding dips on sporadic outcrops, which are necessarily discontinuous. Chargeability measurements from IP data can also help with the possible detection of altered rocks that contain sulfide minerals. Furthermore, when supplemented by field measurements, continuous data sets can have ancillary uses in the development of a deposit, such as geotechnical applications. In this study, we examine variables that may influence AEM and ground resistivity/IP responses at the Canadian Malartic camp with the aim of using such data to derive useful structural information.

Geologic background for the Canadian Malartic district

The Canadian Malartic district is located south of the CLLDZ, a major crustal break that marks the boundary between the Abitibi and Pontiac Subprovinces of the Superior craton. The main metamorphosed Archean rock types include sediments (hereafter called the Pontiac

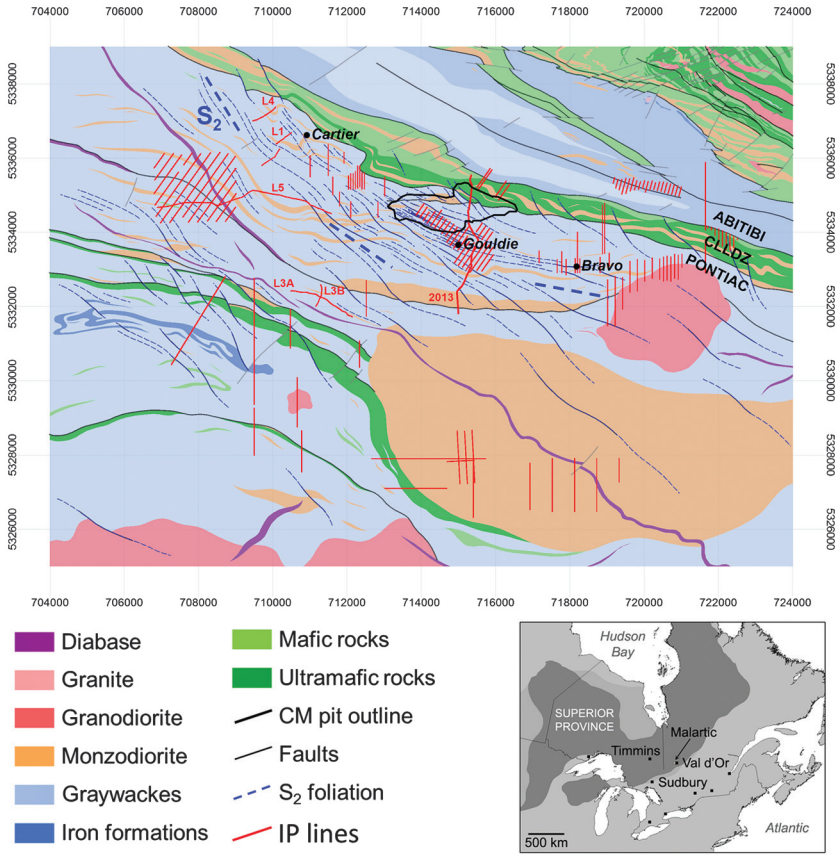

Figure 1. Geologic map of the Canadian Malartic district (modified from Perrouty et al., 2017). The main foliation orientation varies from the northwest–southeast to the west-northwest–east-southeast between the west and east sides of the Canadian Malartic district. Its intensity is stronger in the vicinity of the deposit. CLLDZ is at the boundary between the Abitibi and Pontiac Subprovinces. Historic and recent resistivity/IP surveys are shown as the red lines (with the 2016 survey marked by line numbers L1, L3A, L3B, L4, and L5). For the survey parameters, refer to Table 1. The solid black polygon shows the outline of the 2013 Canadian Malartic open pit. The locations of Cartier, Gouldie, and Bravo zones are depicted by their labels on the map.

group), mafic-ultramafic volcanic flows, and quartz-monzodiorite intrusions (Figure 1). They are overlain by a 0–50 m thick layer of Quaternary sediments (e.g., till, Figure 2a). In the Canadian Malartic deposit, all of the Archean lithologies underwent hydrothermal alteration and host gold mineralization (Helt et al., 2014; Gaillard et al., 2018). The structural controls on the mineralization were extensively described by Derry (1939), De Souza et al. (2016), and Perrouty et al. (2017) and consist of two major features visible in the open-pit mine: (1) an east–west fault zone that lies along the southern contact between a quartz-monzodiorite body and its host Pontiac group and (2) a series of northwest–southeast high-strain structural corridors within fold hinges. At the district scale, these fold hinges were interpreted to represent the most favorable settings for quartz-monzodiorite intrusions and spatially associated gold occurrences (Perrouty et al., 2017). Fold hinge zones result in a higher variability of bedding orientation and therefore represent structurally complex zones. They are typically a favorable setting for quartz-monzodiorite intrusion in the Canadian Malartic district (e.g., Figure 2c), for hydrothermal alteration (e.g., Figure 2e; Blacklock, 2015), and for gold mineralization (e.g., the northwest–southeast high-strain zone, De Souza et al., 2016; Perrouty et al., 2017).

METHODS

The airborne and ground geophysical data used in this paper come from four different sources. Each of the data sets and their associated processing are described in the following sections.

Airborne frequency-domain electromagnetic survey

A frequency-domain (FD) helicopter electromagnetic survey at Malartic, near the CLLDZ, was conducted in 2006 (Figure 3) with the purpose of detecting conductive zones that might be associated with mineralization and to map the geology of the Canadian Malartic district. The survey included data from a multicoil (coaxial and coplanar), multifrequency (877, 1128, 5087, 7166, and 56,110 Hz), electromagnetic system known as the DIGHEM (Fraser, 1978). The north–south survey lines had a spacing of 100 m at a nominal system elevation of 30 m above ground. The survey also included magnetic data, which was used together with regional surveys, to refine the geologic map of the area (Perrouty et al., 2017). For this analysis, the EM data were reprocessed and an apparent resistivity map was created with an algorithm that calculates the 1D homogeneous half-space resistivity at each point using the inphase and quadrature components from the multifrequency (877, 7166, and 56,110 Hz) coplanar data. The map in Figure 3b shows the resulting apparent resistivity. Because of the half-space model used in this calculation, the apparent resistivity at each point represents an integrated value for (approximately) the top 100 m below the surface. Notable in the results is the mining pit (solid black outline) and the surrounding vicinity to the south, characterized by a very low resistivity zone (<100 ohm-m), which is due to water saturation in the tailing ponds and mining areas that predate the survey (blue cross-hatched areas). This data set was used mainly to validate the results of the resistivity

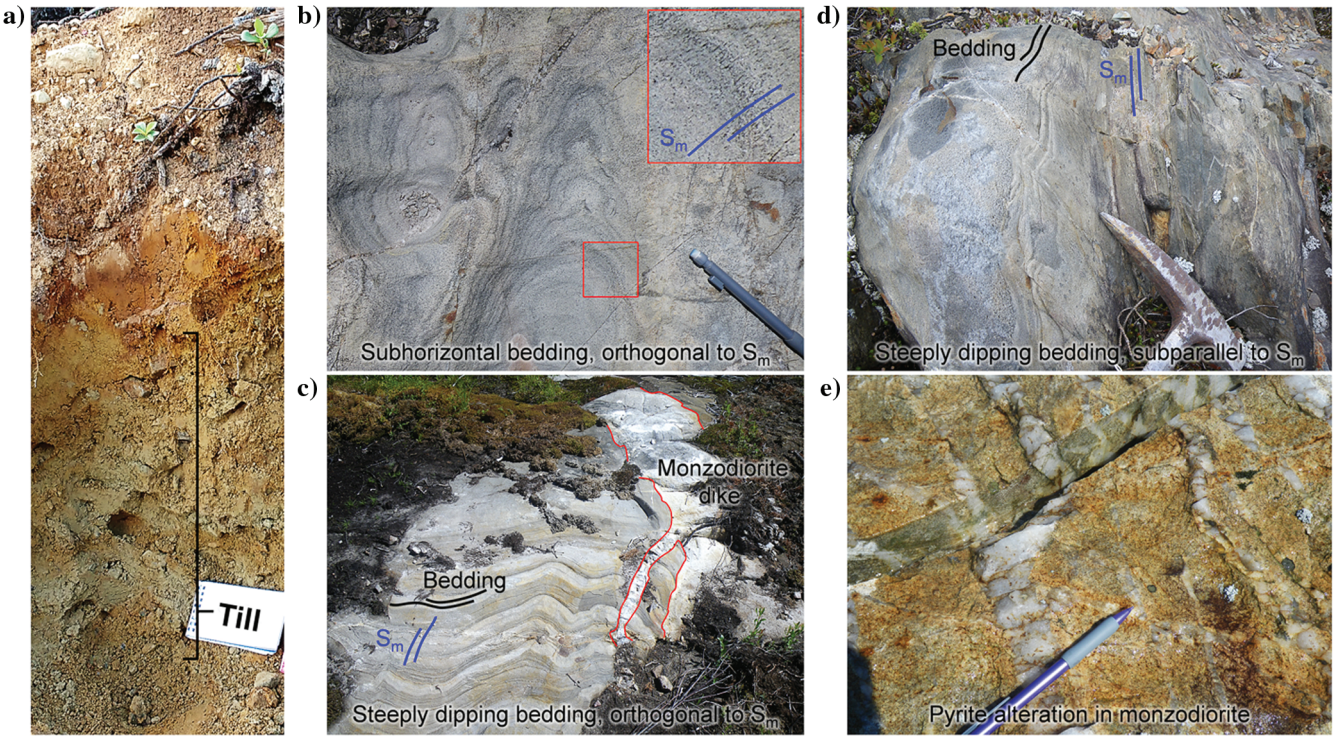

Figure 2. These photographs illustrate some of the main geologic variables that affect AEM and ground IP response in the Canadian Malartic district. (a) Till (photograph courtesy of Caroline E. Taylor). Quaternary sediments (till, deepwater mud, shallow-water sand, etc.) represent more than 90% of the material that overlies the Archean bedrock. The black line highlights the 50 cm thick till cover on top of bedrock. (b) Subhorizontal bedding and steeply dipping foliation (i.e., fold hinge). The rounded irregular patterns are a result of interference between the bedding and the topography. Note in the two insets that biotite abundance marks the bedding and biotite orientation marks the main foliation (denoted as S_m). (c) Steeply dipping bedding orthogonal to the steeply dipping main foliation (i.e., fold hinge). Note the presence of quartz-monzodiorite dikes within the fold hinges. (d) Steeply dipping bedding subparallel to the main foliation (i.e., fold limb). (e) Pyrite alteration in the quartz-monzodiorite dike associated with quartz-carbonate-biotite-microcline-albite veins in the Cartier zone (Blacklock, 2015).

compilation of historical ground data (described in the next section) and to correlate with the surficial coverage in the Malartic district.

Historical resistivity/IP surveys

Additional data from 13 resistivity/IP surveys were retrieved from the publicly available archives of the Ministère de l'Énergie et des Ressources Naturelles du Québec (MERNQ). These historical surveys were collected from 1982 to 2005 by various contracting companies for different exploration projects within the Malartic district (Figure 1 and Table 1). The surveys were retrieved as public reports containing scanned maps with values of resistivity and chargeability in pseudosections. In addition, a single resistivity/IP line was collected specifically for this project in 2013 and was available for this analysis.

The historical surveys are a mix of time-domain (TD) and FD data with varying line spacings, transmitter/receiver configurations, survey parameters, and different measurement units for the chargeability (mV/V, ms, percent frequency effect [PFE], mrad). The process of compiling this disparate data into a single data set useful for analysis consisted of retrieving the data from the MERNQ archives, digitizing the data, georeferencing the positions, and reprocessing some of the survey lines. Subsequently, the IP and resistivity data from each of these surveys were inverted using the image2DTM (Abitibi Geophysics Inc., Val d'Or, Canada) 2D modeling algorithm to produce depth sections of resistivity and chargeability with cell sizes of 12.5 m in each dimension. Finally, a careful leveling of the results from the different surveys had to be implemented before the resistivity and chargeability values could be displayed on a single compilation map. This leveling stage is important because typically a resistivity/IP survey is meant to be interpreted on its own. Combining multiple surveys of different vintages necessarily involves leveling them to make the chargeability values comparable between the different surveys. This leveling was done in one of three ways:

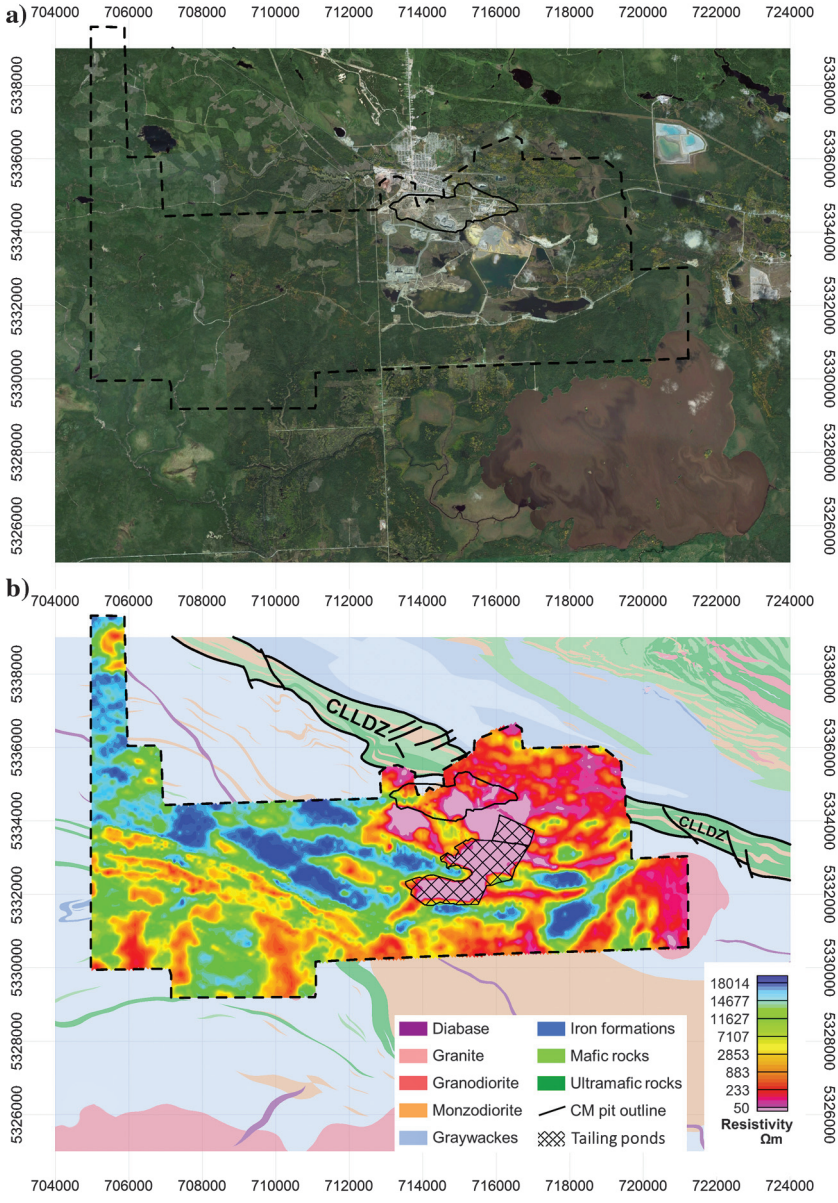

Figure 3. (a) Satellite map of the Canadian Malartic district (Map data: Google, Landsat 2010). The dashed black polygon represents the area investigated by an AEM survey from 2006. The survey covers an area near the town of Malartic close to the CLLDZ. The line direction is north–south with spacing of 100 m and average sensor height of 30 m above the ground. A small section over the current Malartic pit (the black polygon) has infill lines, resulting in an area covered by 50 m line spacing. (b) Apparent resistivity map calculated from the multifrequency (877, 7166, and 56,110 Hz) coplanar AEM data. This represents an integrated average resistivity for the shallow subsurface (<100 m depth). The area marked with the cross-hatched polygon is heavily influenced by mining-related activities, such as the tailing ponds, and it shows very low resistivities due to water saturation.

1) In cases in which there was an overlap area between two or more surveys, this overlap was used to provide a reference point to bring the surveys into the same comparable chargeability range.
2) In cases of no overlap, neighboring surveys spanning identical lithologic units were used to level chargeability values.
3) For surveys with different measurement units (mV/V, ms, PFE, mrad), and where methods (1) and (2) were inapplicable, an empirical rule of thumb was used to convert between units (Table 2). Historically, different units have been used to measure and report chargeability from geophysical surveys. Although each unit quantifies the same physical parameter, comparison of data in different units is not trivial because conversion among them depends on exact knowledge of the specific survey parameters (timing windows or frequencies) used in each survey — information that is not available in the case of older historical data. Approximate relations like the one in Table 2, arrived at from studies of the same target with different methods, can be used to compare results between dissimilar IP surveys (Smith, 1980; UBC GIF group, personal communication, 2016).

In the final step, all the leveled data were gridded together using Geosoft Oasis Montaj to produce a compilation volume of resistivity and chargeability that is shown in Figure 4.

2016 resistivity/IP survey

In May 2016, five new resistivity/IP lines in the Canadian Malartic district were collected to supplement the available historical surveys. These additional lines were planned to focus on the relationship between resistivity/chargeability and structure, in addition to in-filling some of the gaps in the existing resistivity/chargeability coverage (Figure 1). The new survey lines were chosen to coincide with areas where previous measurements provided detailed structural information. In this way, geophysical results could be interpreted in light of structural variations. The survey was undertaken using a gradient array configuration. The receiver dipole length was 25 m, with survey lines (transmitter dipole length) varying from 800 m to 5 km in extent. These lines were inverted using the UBC GIF DCIP3D algorithm (UBC-Geophysical Inversion Facility, 2014), with a cell size of 5 m in each dimension. The results were combined with the leveled historical surveys and gridded into a single compilation volume (Figure 4).

Outcrop scale resistivity measurements

Apparent chargeability and resistivity measurements were collected in a TD survey at the meter scale on several outcrops in the Canadian Malartic district, including the Gouldie zone (Figure 1). Gradient array soundings of apparent resistivity with an electrode spacing of 50 cm were conducted on even rectangular grids of 50 cm station spacing (Bérubé et al., 2017). At the Gouldie zone, soundings were performed using two orthogonal orientations. A

Table 2. A comparison of different chargeability units in FD and TD.

	Units of measurement			
	TD		FD	
	mV/V	PFE	Milliradian (mrad)	Millisecond (ms)
Chargeability (M)	10	1	7	7

Table 1. Relevant parameters of IP surveys in the compilation.

Survey	Year	Units	TD or FD	Survey type	Line spacing (m)	*N*	*a* (m)
GM38489	1982	ms	TD	Pole-dipole	100	1	50
GM39467	1982	ms	TD	Dipole-dipole	120	1-3	30.5
GM40516	1983	ms	TD	Dipole-dipole	60	1-5	30.5
GM40924	1983	ms	TD	Dipole-dipole	120	1-3	61
GM41099	1984	ms	TD	Dipole-dipole	60	1-3	30.5
GM44394	1987	mrad	FD: 1 Hz	Dipole-dipole	150	1-3	50
GM45871	1987	mrad	FD: 1 Hz	Dipole-dipole	1000	1-4	30.5
GM55481	1997	mrad	FD: 1 Hz	Dipole-dipole	600	1-5	50
GM48278	1988	PFE	FD: 0.25–4 Hz	Dipole-dipole	100	1-6	25
GM53309	1995	mV/V	TD	Dipole-dipole	200	1-6	50
GM55482	1997	mV/V	TD	Dipole-dipole	800	1-5	25
GM61225	2004	mV/V	TD	Dipole-dipole	1 line	1-6	50
GM61642	2005	mV/V	TD	Dipole-dipole	200	1-6	50
Abitibi-2013	2013	mV/V	TD	Dipole-dipole	1 line	1-35	40
CMIC-2016	2016	mV/V	TD	Gradient	Variable	—	25

Note: The parameter *a* is the receiver dipole spacing, and *N* is the offset between the receiver and transmitter electrodes in integer multiples of *a*.

first survey was undertaken using an east–west-trending electrode layout. A second overlapping survey was conducted on the same grid using a north–south-trending electrode layout. An IRIS Elrec Pro receiver (12 measurement channels and 20 time windows), a Huntec Lopo transmitter (2 s on-off time), and stainless steel electrodes were used to collect the field data.

For reference, the different data sets used in this study, along with their sources and derived products, are summarized in Table 3.

RESULTS

In this section, the resistivity and chargeability data are analyzed with respect to several different parameters to try and understand the character of some of the anomalies and the implications for interpreting these data in the context of structure and mineralization.

Airborne and ground resistivity

There is considerable overlap between the AEM and the ground resistivity/IP compilation. Because the two data sets operate at different scales and use different methods, it is of interest to compare the ground and airborne resistivity in places where there is common coverage. In particular, because the airborne data are of uniform coverage and the ground data are a compilation of different survey patches, a good correspondence between the near-surface inverted ground resistivity and airborne apparent resistivity at common locations can give confidence in the quality of the compilation.

The airborne apparent resistivity is calculated from multifrequency coplanar data at 877, 7166, and 56,110 Hz. Assuming an average ground resistivity of approximately 2000 ohm-m, the plane-wave skin depth is approximately 100–850 m at these frequencies, but for a magnetic dipole source, the depth sensitivity is consider-

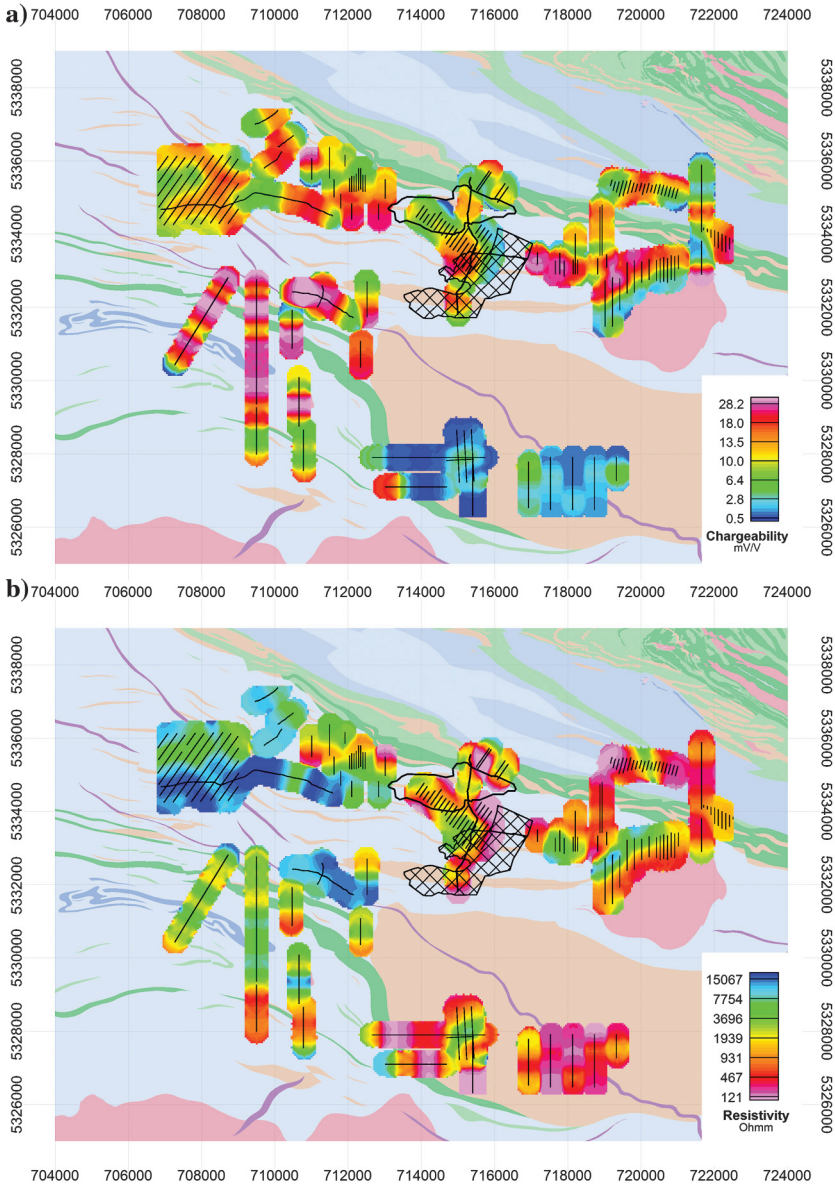

Figure 4. Surface slices from the compilation of historical and recent resistivity/IP surveys. For the geology legend, refer to Figure 1. The plots are (a) chargeability and (b) resistivity values at the surface. These compilations are produced by combining results from inversions of historical and recent surveys. The compilations cover depths of up to 300 m below the surface. (See the text description for leveling of chargeability. No significant leveling was necessary for the resistivity data.) There are a total of 15 surveys, ranging from 1982 to 2016. The black lines are the individual survey lines, the pit is shown as a black polygon, and the main tailing pond is shown as the cross-hatched area.

ably less, so that FD helicopter AEM systems are rarely sensitive to conductive features greater than 80 m in depth, and only up to 100 m in the most ideal cases (Beamish, 2004; Tølbøll and Christensen, 2007). Furthermore, the 1D apparent resistivity calculation used here for the airborne data, provides a single depth-integrated resistivity value at each position. For ground measurements, depth sensitivity is dependent on the geometry of transmitter and receiver electrodes, but for most of the surveys in this analysis (for survey parameters, see Table 1), the sensitivity is limited to the top 200 m below the surface due to the generally small array sizes/geometries that were used. Where there is conductive ground cover (such as water-saturated mine tailings), the depth of investigation decreases significantly because the currents in the ground (either inductively induced as in the airborne survey or galvanically injected as in the ground survey) are generally confined within the conductive zone.

A comparison of airborne and ground resistivity at colocated points is shown in Figure 5. To create this comparison, both data sets were averaged around the same positions with an averaging radius of 100 m in the lateral directions and 50 m in depth. This averaging radius is necessary, and it represents a common spatial scale for comparison of these two types of data because a comparison is only meaningful at equivalent scales. The correlation plot of Figure 5 shows that there is a good connection between ground and airborne resistivity when comparing coverage in areas not in the immediate vicinity of the pit or tailing ponds. The points that do not show a good correlation, defined where there is at least a factor of 10 difference between the ground and airborne resistivity values, are shown in the red and are considered outliers. An examination of these outlier points indicates that they are all within the vicinity of the tailing ponds and the pit. The ground resistivity data at these locations are derived from a 1982 survey, whereas the airborne data are derived from 2006. Between these dates, mining activities including the pit and tailing ponds have contributed to large changes in the surface resistivity, evident in the discrepancy between the two data sets. The good correlation (correlation coefficient of 0.78) between airborne and ground resistivity away from the mine area, gives confidence in using the resistivity/IP compilation for further analysis of structure and geology in the Canadian Malartic district.

Airborne resistivity, topography, and surficial coverage

Topographic relief in the Canadian Malartic district ranges between 290 and 400 m with an average elevation of 320 m above mean sea level (Figure 6a). Topography is commonly related to ground cover as well as water saturation; therefore, it is important for interpreting resistivity variations. The main topographic feature is a northwest–southeast-trending zone of high elevation (>350 m), which terminates at the low-lying (<300 m) Lac Fournière area to the southeast. This high-elevation corridor, with thin overburden cover (<1.5 m, Figure 7d), is associated with very high resistivities (Figure 6b). Within this zone, however, there are two distinct conductive parallel bands (shown with the black arrows in Figure 6b) that traverse the southern slope of the high-resistivity, high-elevation zone. These two parallel bands correspond closely to the northwest–southeast-trending ultramafic layers depicted in the geology map in Figure 1. The talc-chlorite composition of these ultramafic rocks makes them very incompetent and permeable, which likely increases their apparent conductivity in areas where they are water saturated. In addition, several prominent conductive features can be related to the presence of water in low elevation areas. For example, in the southwest corner of survey coverage (Figure 6b), the main north–south-trending low-resistivity features closely follow the water courses. The most conductive regions (<100 ohm-m), however, correspond to mining-related activities, and in particular, the tailing ponds (i.e.,

Table 3. List of various data sources and their derived products used for this study.

Data	Source	Derived product
Historical resistivity/IP surveys	MERNQ — Table 1 lists the individual survey details sorted by year	Inverted resistivity and chargeability
2016 resistivity/IP survey	Collected for this study by the authors, with support from Abitibi Geophysics Inc. (Val d'Or, Canada). Table 1 lists the survey details under the "CMIC-2016" survey	Inverted resistivity and chargeability
Topography data	SRTM data, 1 arc second resolution recovered from the Geosoft Public Data Access Protocol (DAP) server	Contours of elevation
Overburden data	3731 drillhole logs from the Canadian Malartic Mine, 555 till samples from MERNQ, 27 till samples from Taves (2016), and 345 outcrop sample data from Perrouty et al. (2017)	Gridded overburden thickness map
Structural data	1068 individual field measurements on outcrops from the Canadian Malartic and Perrouty et al. (2017)	Gridded map of the bedding orientation and the variance of the bedding
Airborne electromagnetic data	FD helicopter electromagnetic survey (DIGHEM) conducted in 2006, provided by the Canadian Malartic Mine	Apparent resistivity
Outcrop-scale resistivity/IP survey	Bérubé et al. (2018)	Apparent resistivity and chargeability
Surficial geology	Quaternary geology coverage of the Canadian Malartic district from Veillette (2004)	—
Gold concentration	Data provided by the Canadian Malartic Mine	Gridded map of gold concentration in Pontiac metasedimentary rocks

water-saturated muds or brines) to the south of the mining pit (shown as the cross-hatched area).

Leaving out the tailing ponds and the area in the immediate vicinity of the Canadian Malartic open pit, analysis of airborne apparent resistivity with topography shows that the lowest and highest elevations are exclusively associated with the lowest and highest resistivities, respectively, and there is a positive correlation between topography and resistivity. This is made clear in Figure 6c in which the resistivity within each 10 m elevation interval is averaged and plotted against the elevation.

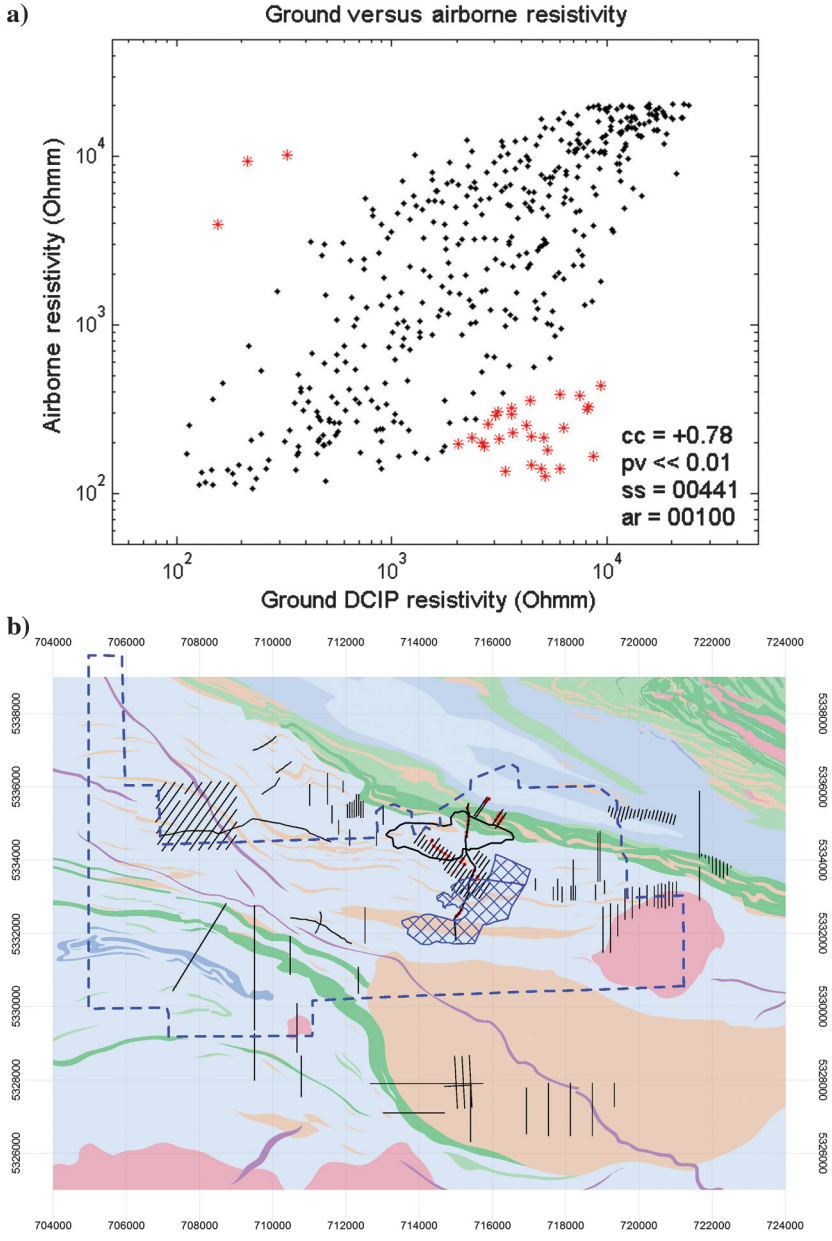

Figure 5. (a) Correlation of ground and airborne resistivity values measured at colocated points, with an averaging radius of 100 m in the lateral directions and 50 m in depth, along with the calculated correlation coefficient and p-value. The p-value is a measure of confidence in the correlation. It is the chance that such a correlation coefficient would exist for two entirely uncorrelated variables. In this case, the p-value is far below 1% (cc, correlation coefficient; pv, p-value; ss, number of samples in the correlation analysis; ar, averaging radius in meters). The points that do not show a good correlation are plotted as the red stars. In each case, there is at least a factor of 10 difference between the ground measurement value and the corresponding airborne measurement for these outliers. (b) This map shows that the outlier points — shown in red — are all within the vicinity of the tailing ponds and the pit. The reason for this is most likely that the mining activity has significantly altered the ground resistivity in the time between the ground survey (1982) and airborne data (2006) at these locations. The airborne survey coverage is shown as the dashed blue line.

The airborne apparent resistivity, which is sensitive to the shallow subsurface (<100 m), is also considerably affected by the surficial coverage. This ground cover has a thickness of a few centimeters up to 50 m (Figure 7d), and it is composed mainly of unconsolidated sediments (river, shallow water, deep water) and glacial deposits in the Canadian Malartic district (Veillette, 2004). There are also sporadic bedrock outcrops. Figure 7f shows these components together with the contours from airborne resistivity. In general, the relation between the airborne apparent resistivity and ground cover can be divided into three zones:

1) Very low resistivities (conductive zones) that are associated with the tailing areas and mining-related ground disturbances near and to the south of the pit. In addition to these, the clay-rich deepwater sediments and muds, mainly to the northeast of the survey area, show the lowest resistivities.
2) Mid-range resistivities are well-correlated with surficial till and sand coverage (shown as the green unit in Figure 7f).
3) High resistivities correspond to areas with very thin ground cover and, in particular, the patches of outcrops.

The maps in Figure 7 demonstrate a broad correspondence among airborne apparent resistivity, bedding orientation variance, surficial cover, and topography. These maps exhibit a notable northwest–southeast-trending feature (denoted between the dashed red lines) that corresponds to an area of low structural complexity, high resistivity, and a topographic high that is covered with a thin layer of glacial till deposits. Similarities between these data sets suggest that they are related to each other, with Archean bedrock structures controlling the topography (due to preferential erosion), which in turn is controlling the Quaternary sedimentation. These three interrelated variables all affect the apparent resistivity to some degree but all derive from the same initial feature: the variation of bedrock structural orientations. Therefore, the airborne apparent resistivity, in areas of thin cover, could be a potential indirect marker of geologic structures in the Canadian Malartic district.

Ground chargeability, resistivity, and structure

The compiled inverted ground chargeability and resistivity is less continuous than the airborne

resistivity coverage, but it does include some areas outside the airborne survey area. Chargeability anomalies are commonly used for detecting the presence of sulfide minerals during exploration programs (Ford et al., 2007). In the Canadian Malartic district, hydrothermal alteration and sulfide minerals (mainly pyrite and pyrrhotite) are spatially associated with quartz-monzodiorite dikes and fold hinges (Blacklock, 2015; Perrouty et al., 2017). In metasedimentary rocks, Bérubé et al. (2018) show that chargeability anomalies are strongly controlled by mineralogical texture (i.e., the surface of contact between the pore water and the sulfide minerals) and that strong proximal alteration may result in negative chargeability anomalies. Positive or negative chargeability anomalies are therefore expected to be observed in mineralized rocks. As an example, Figure 8 shows the near-surface chargeability for two lines that cross folded quartz-monzodiorite dikes in the northwest of the Canadian Malartic district, near the Cartier Zone gold occurrence. These two lines are marked L4 and L5 on the map of Figure 1. What these lines show is that there is a correlation between the elevated chargeabilities and the folded regions of quartz-monzodiorite dikes that contain significant (i.e., >1%) sulfide mineral concentration. Chargeability anomalies, up to five times the background value, are particularly pronounced near fold hinges in the quartz-monzodiorite rock, potentially due to thickening of the unit and increased pyrite concentration in contact with the pore water in these structurally complex zones.

Resistivity variations associated with hydrothermal alteration in the Canadian Malartic camp can be quite subtle, but resistivity can potentially be used to identify certain structural features. For example, L4 (Figure 1) was specifically chosen because it proceeds along a uniform variation of bedding orientation from subvertical to subhorizontal (Figure 9a). Surface resistivity for this line shows a steady decrease from the southwest toward the northeast. The depth-averaged resistivity along the line (Figure 9c) shows a clear decrease as the bedding orientation changes from vertical to horizontal. This is consistent with the result in Figure 7 that shows an area of very high resistivity within a northwest–southeast corridor, coincident with an area of subvertical bedding.

The potential relationship between resistivity and bedding orientation suggested in Figure 9 can be further examined by looking directly at the correlation between these two parameters, measured at the same locations, over the much larger area for which measurements are available. In the Canadian Malartic district, 1068 bedding dip measurements are gridded by kriging with a cell size of 100 m. Figure 10a highlights the northwest–southeast corridor (i.e., the subvertical bedding), which is also seen in other data layers (Figure 7). In contrast, the area around the mine is dominated by much more chaotic bedding dip variations (Figure 10b). To look for correspondence with resistivity, the compilation created from the latest inversion of historical resistivity/IP data is used. Colocated point pairs are created by average and standard deviation of the bedding dip and resistivity around a given point within a radius of 100 m. Inverted resistivity values at depths greater than 25 m are used; this is to minimize the effects of near-surface resistivity variations due to surficial cover. Correlations between bedding and average resistivity produced in this way are plotted in Figure 10c (left axis), and they show that, in general, as the bedding becomes more vertical, the resistivity values and the variation in resistivity values increase. This is further demonstrated by examining the red curve, which shows the standard deviation of resistivity for different bedding dips (Figure 10c, right axis). A simple interpretation for this observation

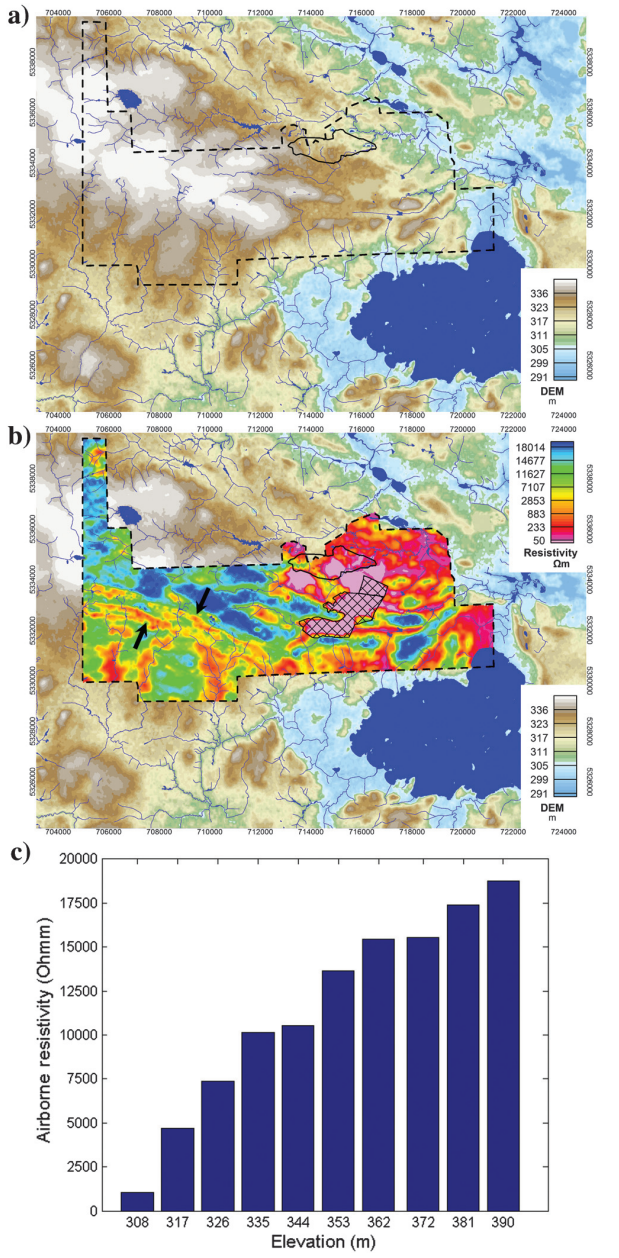

Figure 6. (a) Topography in the Canadian Malartic district (1 arc second resolution recovered from the Geosoft Public DAP Server). DIGHEM survey coverage is shown with the dashed black polygon, whereas water bodies, rivers, and streams are in deep blue. (b) Airborne resistivity and Malartic topography. Two distinct conductive parallel bands, marked by the black arrows, correspond closely to ultramafic bedrock in this area (see Figure 1). The conductive cross-hatched area marks the water-saturated tailing ponds. (c) Depiction of correlation between resistivity and topography. The bar plot shows the average resistivity within each 10 m elevation interval centered around the indicated elevations on the *x*-axis (the immediate vicinity of the pit and tailing ponds are masked out in this analysis). In some places, the association of low elevations with low resistivity can be explained by looking at map (b), which shows the rivers and water bodies overlaid on the resistivity map. Several prominent conductive features are related to the presence of water in the local low-elevation areas. For example, in the southwest corner of the survey coverage, the main north–south-trending low-resistivity features follow the water courses closely.

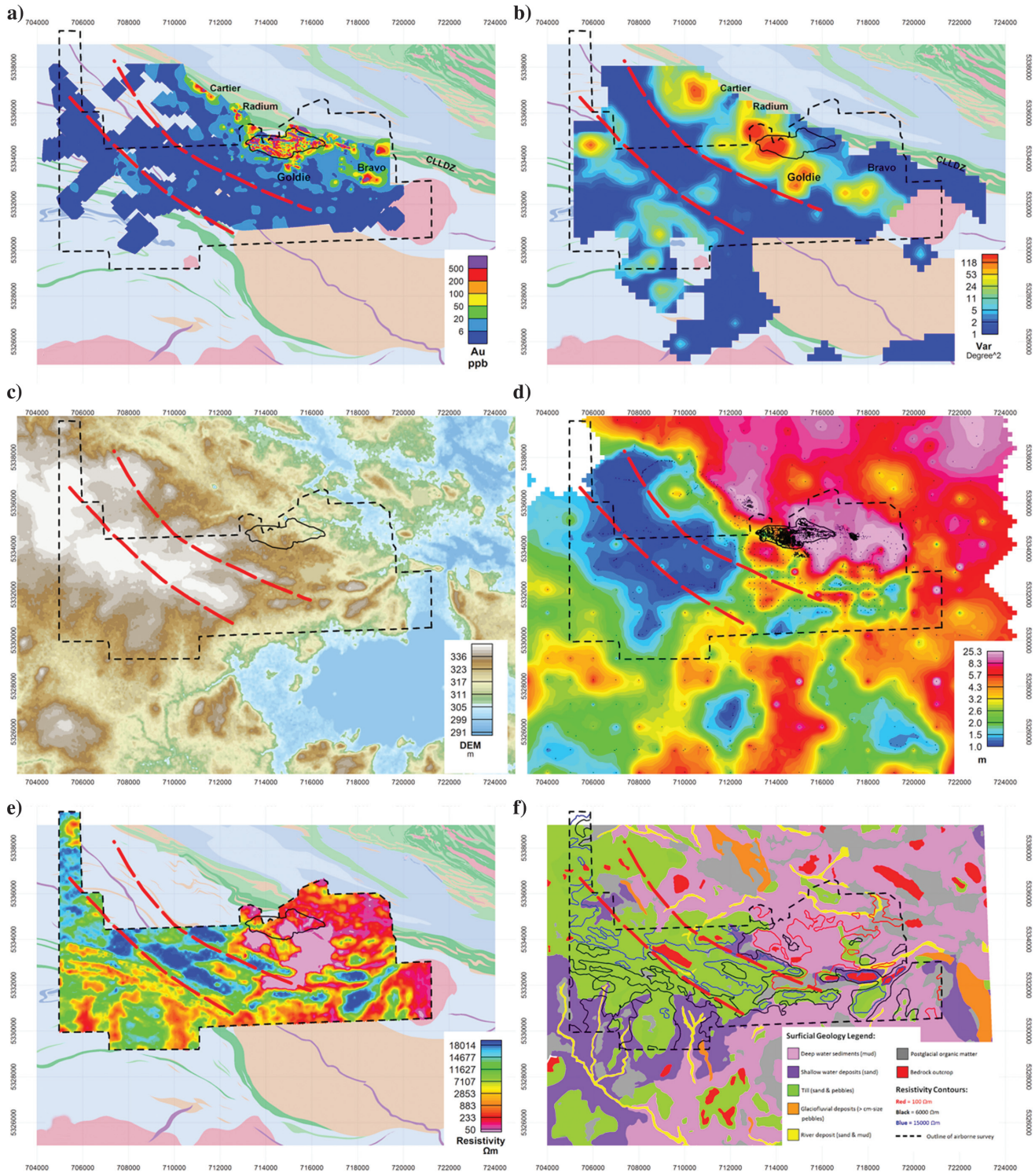

Figure 7. Comparison of (a) gold concentration in the Pontiac group, (b) bedding dip variance calculated from field structural measurements, (c) topography (1 arc second resolution recovered from the Geosoft Public DAP Server), (d) average cover thickness produced by gridding (200 m cell size) the measurements of overburden in the field located at the black dots. The overburden data are a compilation of 3731 drillhole logs from the Canadian Malartic, 555 till samples from MERNQ, 27 till samples from Taves (2016), and 345 outcrop sample data from Perrouty et al. (2017), (e) airborne apparent resistivity and (f) Quaternary geology coverage of the Canadian Malartic district (modified after Veillette, 2004) with the contours from the airborne resistivity superimposed. The most conductive contour follows the tailing areas and other mining-related ground disturbance near the pit. Outside of those areas, the most conductive regions correspond to the surface coverage of clay-rich deepwater sediments and mud. The mid to high resistivities are well-correlated with the surficial till and sand coverage. The sporadic outcrops display very high resistivities. The corridor marked by the dashed red lines outlines the correspondence between these various data around the Canadian Malartic deposit. See the text for discussion.

is the presence of an anisotropy of apparent resistivity due to the relative orientation of different survey lines with respect to the bedding geometry: Subhorizontal bedding results in a more isotropic resistivity response whatever the orientation of the survey lines, whereas subvertical bedding results in a higher resistivity response if the survey line is perpendicular to the strike of the bedding and a possibly lower resistivity response if the survey line is parallel to the strike of the bedding. Therefore, subvertical bedding with a variable strike due to folding will result in a higher standard deviation of the apparent resistivity.

To test this interpretation, we collected resistivity/IP data along orthogonal lines in two separate areas of well-defined bedding in the Pontiac group (the locations are shown in Figure 1):

1) The bedding near lines 3A and 3B is homogeneously trending west-northwest–east-southeast, and it is subparallel to the main foliation. Lines 3A and 3B are oriented parallel (east–west) and perpendicular (north–south) to the bedding, respectively.
2) The bedding near the Gouldie zone is open folded, varies from north-northwest–south-southeast to east-northeast–west-southwest trending, and it is at a high angle to the main foliation (Sansfaçon and Hubert, 1990; Perrouty et al., 2017). The orthogonal east–west and north–south survey lines in Gouldie are not exactly aligned with the bedding.

Note the overall 90° difference in bedding orientation between these two areas. In each area, the measurements are collected at different scales and over uniform lithology so as to enable attribution of changes in resistivity to variations in structure. The inverted chargeability and resistivity along lines 3A and 3B are presented in Figure 11a and 11b, whereas the apparent chargeability and resistivity measured over the Gouldie zone are shown in Figure 11c and 11d. Chargeability, which is associated with the total surface area of polarizable mineral grains (e.g., sulfide minerals) in contact with pore water, changes little (less than 5% on average) between lines 3A and 3B (Figure 11a). On the other hand, resistivity, which is affected by the geometry of current flow, is approximately 1.6–2 times higher along the bedding-perpendicular (north–south) line 3B than the bedding-parallel (east–west) line 3A (Figure 11b). At the Gouldie zone, resistivity and IP measurements at the outcrop scale show that apparent chargeability is isotropic in the east–west (5.2 ± 0.2 mV/V) and north–south (5.1 ± 0.5 mV/V) directions (Figure 11c). In contrast, apparent resistivity (Figure 11d) measured in the east–west direction (6753 ± 372 ohm-m) is on average 1.7 times higher than the one

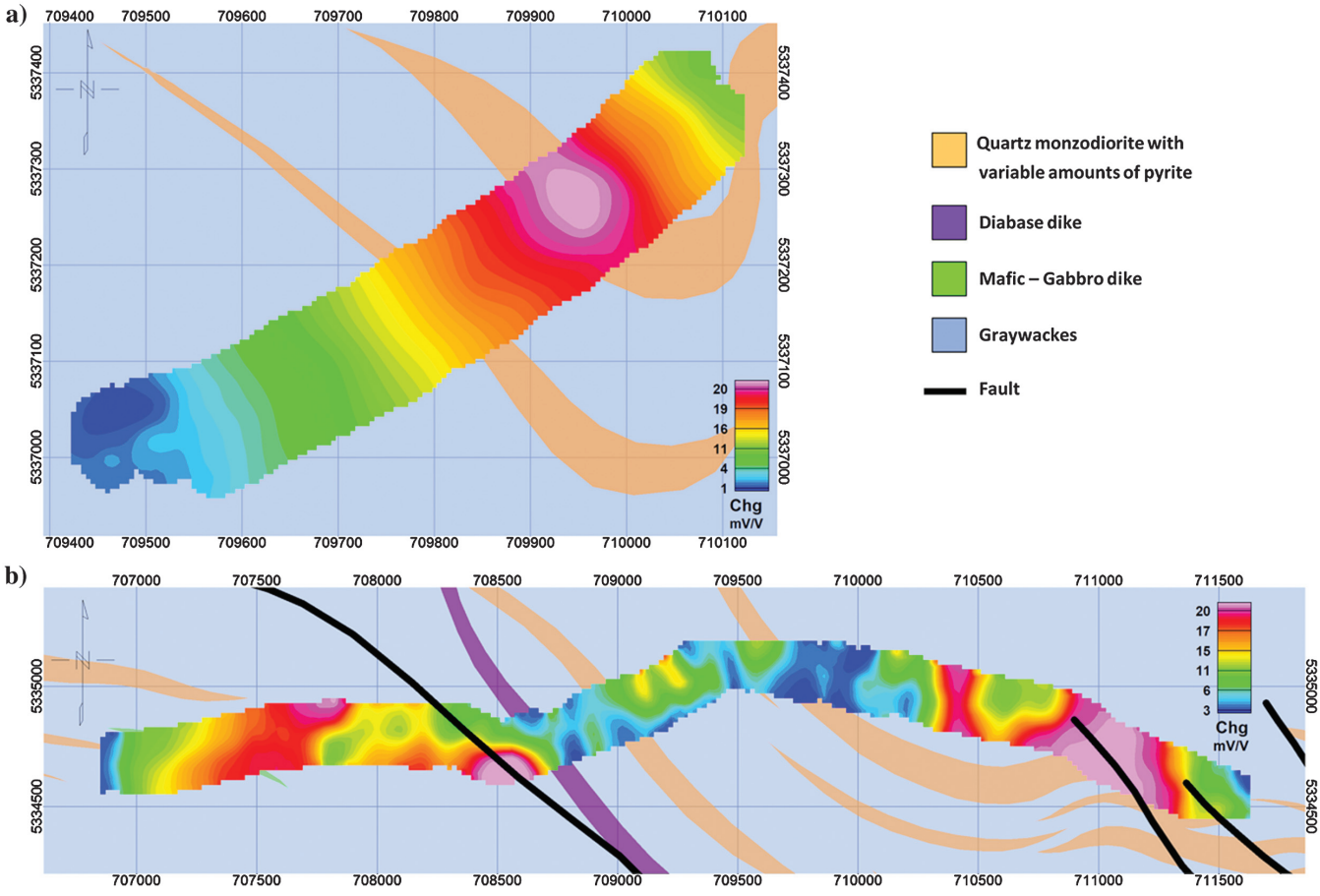

Figure 8. Near-surface chargeability results from (a) line 4 and (b) line 5 of the 2016 survey. These two lines are labeled in Figure 1 (the eastings and northings are shown around the border of the map, and the north is toward the top). On line 4, the chargeability anomaly is associated with hydrothermally altered (rich in sulfide minerals) quartz-monzodiorite dikes near fold hinge. On line 5, the eastern chargeability anomaly is spatially associated with a small foliation-parallel mineralized fault, cross-cutting quartz-monzodiorite dikes. The western chargeability anomaly is associated with altered quartz-monzodiorite within fold hinge. A major fault separates the east and west parts of this line.

measured in the north–south direction (3909 ± 330 ohm-m). These field experiments at different scales validate the presence of structurally controlled resistivity anisotropy in the Pontiac group, and they show that the anisotropy ratio of this property can reach values up to two, when the lines are exactly parallel and perpendicular to the bedding.

To further investigate changes in resistivity associated with structural complexity, the bedding variance and its relationship to resistivity can be examined. The comparison of the raw bedding dip with resistivity (Figure 10a and 10c) suggests that it is not straightforward to assign resistivity ranges to areas with different bedding orientations. However, by defining the bedding variance as the parameter of interest, it can be attempted to assign resistivity ranges to areas of highly variable bedding orientation. In this case, field measurements of bedding angles are used to calculate a variance map that displays areas of structural complexity as zones with high variance (Figure 10b). The variance of bedding at a given point is calculated by taking all the bedding measurements within a radius of 100 m within that point and calculating the variance following the formula: $1/N \sum_i^N (x_i - \bar{x})^2$. The results are then gridded using the kriging method in Geosoft Oasis Montaj. A different method of computing variance is by using the grid mathematics described by Perrouty et al. (2017). The inverted resistivity/IP compilation is then used to look for correlations with bedding variance. Resistivity values from depths greater than 25 m were used for this analysis. For each location with a bedding variance calculation, resistivities from the compilation within a radius of 100 m were averaged to give a colocated mean resistivity. The correlation plot is shown in Figure 10d and shows a trend of decreasing resistivity as the variance of bedding increases within structurally complex zones.

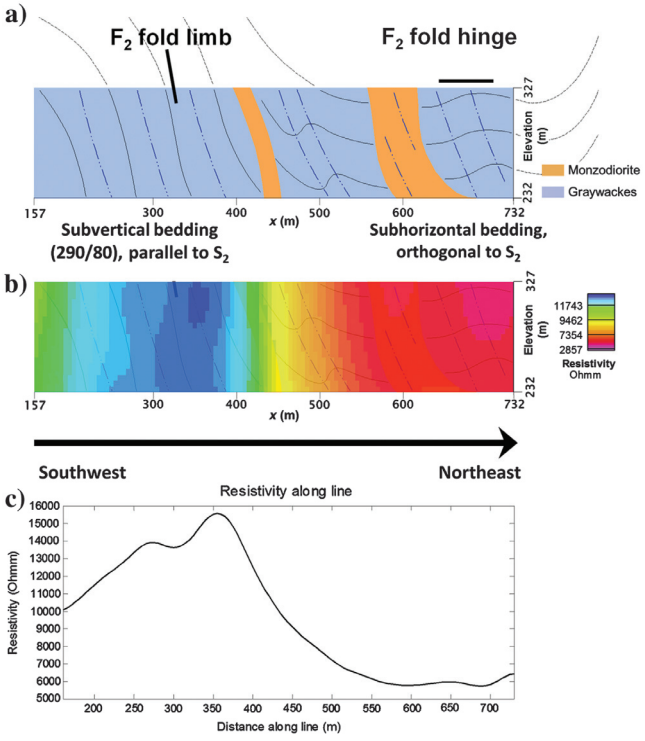

Figure 9. Structure and resistivity results from line 4 of the 2016 survey. This line is labeled in Figure 1. Line 4 was specifically chosen because it proceeds along a uniform variation of bedding orientations from horizontal to vertical. (a) Schematic geologic cross section for line 4 showing a synform fold (modified from Perrouty et al., 2017). (b) Resistivity cross section for line 4 and (c) depth-averaged resistivity along the line, showing the decrease as the bedding orientation changes to horizontal.

DISCUSSION

Comparison of near-surface FD airborne resistivity with topography shows that the lowest and highest elevations are systematically associated with the lowest and highest resistivities observed, respectively. In low-elevation areas, prominent conductive features can be related to the presence of water. Several significant low-resistivity anomalies in areas with thin cover and higher elevation are related to ultramafic bedrock, but, in general, there is a trend toward an increase in resistivity with elevation. For the most part, low values of the airborne apparent resistivity outline the surficial coverage of the Quaternary till and sand. The lowest resistivity values in the airborne data are observed over the tailing areas (mud and water). High resistivity values are commonly observed over outcrops. The airborne data are valuable in mapping Quaternary surficial cover and in this case proved very useful in providing a quality-control check on the leveling and stitching of the disparate historical ground resistivity/IP data. It should be emphasized that the calculation of this apparent resistivity from airborne data is based on a half-space treatment and as such is an integrated value for at most the top 100 m below surface, and it is therefore quite sensitive to surficial cover. In general, there is a broad correspondence among the topography, surficial material, airborne resistivity, overburden thickness, and bedding orientation data. The main characteristic of these maps is a distinct northwest–southeast-trending feature across the district (Figure 7). It is possible that these disparate features are all related to each other, indirectly representing the structural architecture of the Canadian Malartic district.

Petrophysical anisotropy at the outcrop to district scales is poorly documented in the geophysical literature. This study shows that chargeability data can map zones where quartz-monzodiorite dikes are folded, thicker, and therefore contain more sulfide minerals (Figure 8), independent of the survey line orientation. In contrast, resistivity is anisotropic at the district and outcrop scales (>100 m on lines 3A and 3B, approximately 1 m on Gouldie lines) and the apparent values are a function of the survey line orientation relative to the main structures (Figures 9 and 11). The demonstrated presence of anisotropy of resistivity has major implications for future resistivity surveys in deformed terranes where bedrock is exposed or where the surficial cover is homogeneous and well-understood:

1) Apparent resistivity provides a quick first-pass interpretation of the airborne data, but it is mostly sensitive to Quaternary geology (topography and surficial cover) in this case. Given that the conductive overburden will strongly influence this type of data, structural information is most likely to be obtained in those areas that have little to no overburden.
2) Measuring orthogonal ground resistivity/IP lines should be systematically considered to assess possible anisotropy of resistivity and subsequently to interpret the orientation of significant structures.
3) Resistivity variations along a line may be related to lithologic changes or to structural orientation changes. Lithologic interpretation is only valid where the orientation of the lines is consistent relative to regional structures. Similarly, local structural

interpretation (e.g., variance of bedding) is valid when the lines are within the same lithology and the resistivity is estimated at a depth below the influence of conductive overburden.

4) The strength of the anisotropic variation in resistivity will be dependent on the relative orientation of a survey line with respect to the strike of the bedding. Therefore, in general, the correlation of the ground resistivity with bedding orientation will show a much greater variation in measured resistivities in areas with subvertical bedding orientation (Figure 10c).
5) Interpretation of surveys should take anisotropy into account, for example, in the resistivity inversion algorithms. This is particularly relevant for interpretation of modern 3D surveys in which current flow in multiple directions must be considered.

Because structural complexity is closely associated with mineralization, the identification of structurally complex zones is important for exploration. Structural complexity can be quantified with measurement of bedding orientation and calculation of bedding variance maps. Analysis of the ground resistivity compilation in the Canadian Malartic district shows that there is a consistent correlation between increased bedding variance and a decrease in the average inverted resistivity at depths greater than 25 m at a lateral scale of 100 m (Figure 10). Because direct detection of the deposit at Canadian Malartic using geophysics has proved challenging, a potential proxy can be the mapping of structurally complex areas (high bedding variance) associated with mineralization, using ground resistivity.

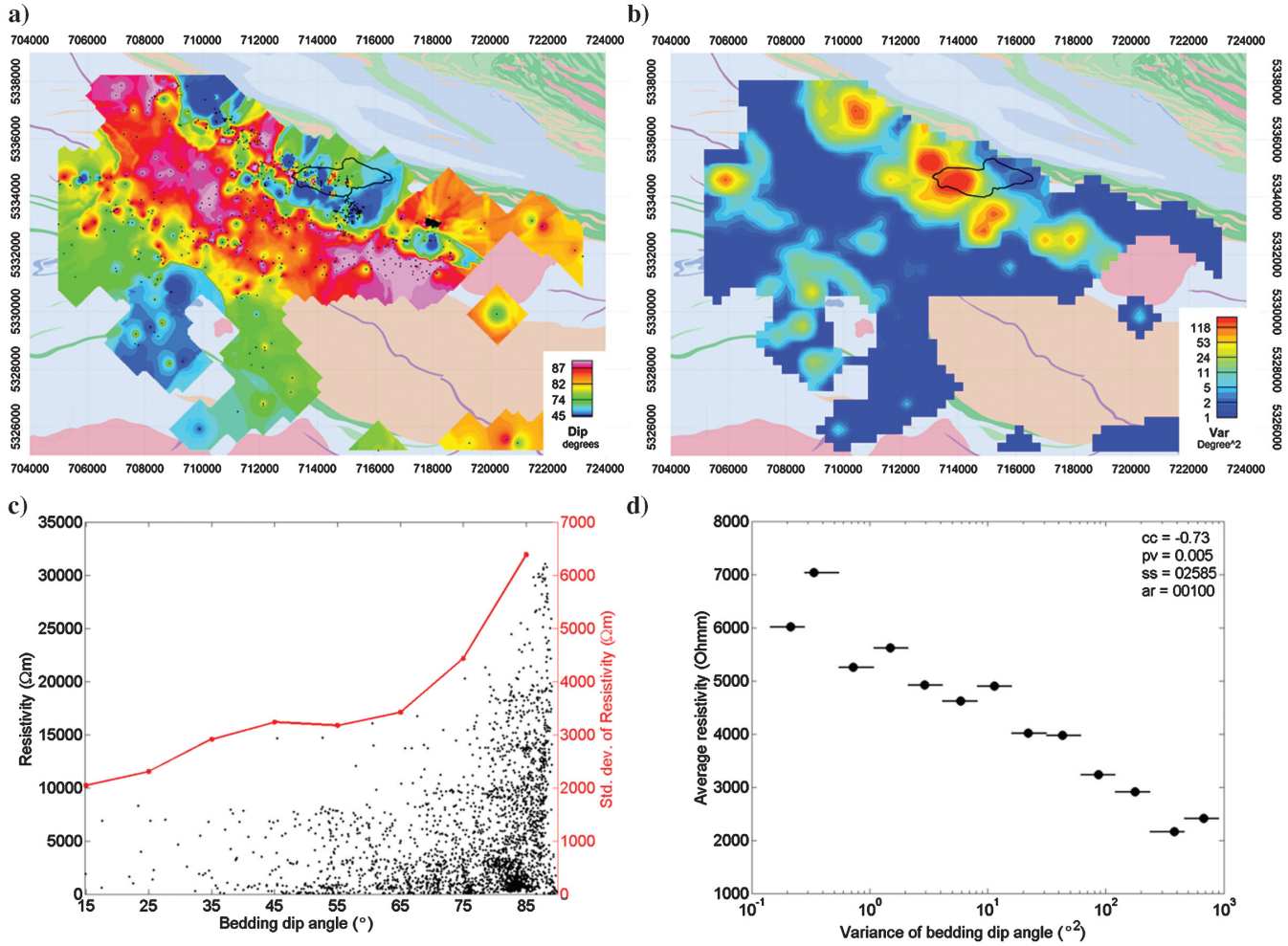

Figure 10. (a) Map of the bedding dip angle created from gridding 1068 individual field measurements on outcrops (shown as the black dots). (b) Gridded map of bedding variance. Structural complexity is signified by those areas with high variances in bedding orientations. (c — left axis) The correlation of bedding dip with ground resistivity compilation. The bedding dip and resistivity are averaged within cell sizes of 100 m. Resistivity at depths greater than 25 m is used. (c — right axis) The standard deviation of resistivity values within 10° bins in the bedding dip angle is plotted. As the bedding becomes more vertical, the variation in measured resistivity values increases. (d) Plot of the correlation between the ground resistivity and the calculated bedding variance. The two parameters are averaged within a radius of 100 m around colocated points. The average resistivity is plotted for logarithmically spaced intervals in the bedding variance. The horizontal bars represent each variance bin, and the dots are the mean variance value in that interval. A correlation coefficient was calculated together with a p-value. The p-value is a measure of confidence in the correlation. It is the chance that such a correlation coefficient would exist for two entirely uncorrelated variables. In this case, the p-value is less than 1% (cc, correlation coefficient; pv, p-value; ss, number of samples in the correlation; ar, averaging radius in meters).

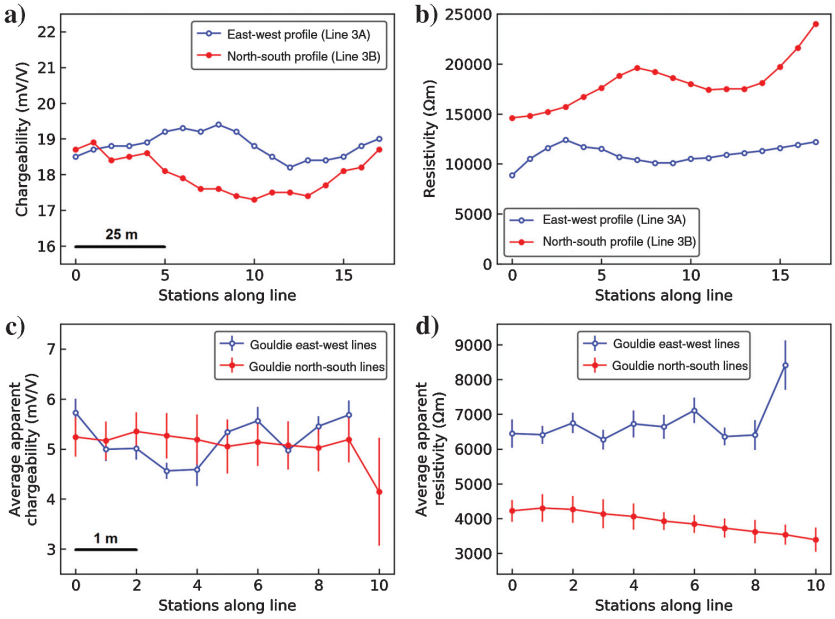

Figure 11. (a and b) Comparison of chargeability and resistivity in the overlap area of two orthogonal lines 3A and 3B, which run, respectively, parallel (east–west) and perpendicular (north–south) to the bedding. The station spacing is 5 m. (a) Chargeability for lines 3A and 3B shows little difference between the two where they overlap. (b) The resistivity along line 3B (perpendicular to the bedding) is on average 1.6–2 times greater than the resistivity along line 3A (parallel to bedding) over the same area. (c and d) Comparison of the apparent chargeability and resistivity measured in the orthogonal directions using the east–west lines and north–south lines at the Gouldie outcrop (see the text for the structural description). The station spacing is 50 cm. (c) The average apparent chargeability is overall constant between the Gouldie outcrop lines. (d) The average apparent resistivity varies by a factor 1.7 between the orthogonal lines of the Gouldie outcrop. Note that resistivity and chargeability values are not comparable between the two surveys (lines 3A and 3B versus Gouldie zone) because they are measured over very different scales.

CONCLUSION

Reprocessing and compilation of historical resistivity and IP data together with more recent surveys, in addition to AEM data and geologic measurements, have yielded a better understanding of the link between geophysical data and structure in the Canadian Malartic district. The main results are as follows:

1) Disparate historical resistivity/IP surveys were recovered from public archives, inverted, leveled, and compiled into a single database for structural analysis. The newly created compilation of historical resistivity/IP was used to show resistivity and chargeability correlations with structures favorable for mineralization.
2) Apparent resistivity, calculated from AEM data, delineates the Quaternary geology at the Canadian Malartic. The shallow depth of investigation together with the 1D nature of the apparent resistivity calculation, which gives a depth-integrated resistivity value, means that the apparent AEM resistivity is quite sensitive to surficial cover. However, these data proved quite useful in validating the leveling and stitching of the ground resistivity/IP compilation.
3) The recent IP data collected in 2016 show that chargeability is elevated in zones where quartz-monzodiorite dikes are folded and thicker, likely due to concentration of sulfide minerals in these areas.
4) The presence of anisotropy of resistivity due to structure (orientation of bedding and main foliation), at different scales, in the Malartic district has been demonstrated. Where the bedding is subvertical, the survey line orientation with respect to the strike of the bedding strongly affects the obtained value of resistivity at outcrop and larger scales (50 cm to 100 m). Measured resistivities can vary by up to a factor of two, over the same location, depending on whether the survey lines are perpendicular or parallel to the strike of bedding. Consequently, obtained resistivity values are much more varied in terrains with subvertical bedding than in those with subhorizontal bedding (Figure 10c). This has implications for survey planning, inverse modeling, and interpretation of resistivity data.
5) In the Malartic district, variance of bedding dip, which defines a measure of structural complexity, is inversely correlated with resistivity: Analysis of the compilation of inverted ground resistivity together with the field structural measurements within a spatial scale of 100 m, shows that an increase in the variance of bedding dip is associated with a decrease in the average resistivity below cover (depth >25 m). This suggests that resistivity can potentially be used as a way to identify zones of structural complexity, which are known to be favorable for mineralization.

ACKNOWLEDGMENTS

We are very grateful to Abitibi Geophysics Inc. for their logistical support during the fieldwork and for providing survey data as an in-kind contribution to the project, in particular, P. Bérubé, who helped with planning the fieldwork and provided inversions of the historical data through the Abitibi Geophysics proprietary software. We thank the Canadian Malartic Corporation for providing logistical support and access to their property and data. We are also grateful for the support of CGG who provided software for the inversion of AEM data. We also thank the subject matter experts and our colleagues involved in the CMIC Footprints project for fruitful discussions and comments on this work. Funding was provided by the Natural Sciences and Engineering Research Council of Canada and the Canada Mining Innovation Council through a grant from the NSERC Collaborative Research and Development Program. This is NSERC-CMIC Mineral Exploration Footprints Project Contribution 178.

DATA AND MATERIALS AVAILABILITY

The source data for this research is a mix of publicly available data and proprietary industry data. The publicly available data can be obtained from the archives of the Ministère de l'Énergie et des Ressources Naturelles du Québec (MERNQ), using the survey names listed on Table 1 of our paper, at the following link: http://sigeom.mines.gouv.qc.ca/signet/classes/I1102_index?entt=LGl=A.

REFERENCES

Beamish, D., 2004, Airborne EM skin depths: Geophysical Prospecting, **52**, 439–449, doi: 10.1111/j.1365-2478.2004.00428.x.

Bedeaux, P., P. Pilote, R. Daigneault, and S. Rafini, 2017, Synthesis of the structural evolution and associated gold mineralization of the Cadillac fault, Abitibi, Canada: Ore Geology Reviews, **82**, 49–69, doi: 10.1016/j.oregeorev.2016.11.029.

Bérubé, C. L., M. Chouteau, G. R. Olivo, and S. Perrouty, Mineralogical and textural controls on spectral induced polarization signatures of the Canadian Malartic gold deposit: Applications to mineral exploration: Geophysics, **84**, this issue, doi: 10.1190/geo2018-0404.1.

Bérubé, C. L., M. Chouteau, G. R. Olivo, S. Perrouty, P. Shamsipour, and R. Enkin, 2017, Spectral induced polarization signatures of altered metasedimentary rocks from the Canadian Malartic gold deposit Bravo zone, Québec, Canada: 30th Symposium on the Application of Geophysics to Engineering and Environmental Problems, Environmental and Engineering Geophysical Society, Expanded Abstracts, 204–208.

Bérubé, C. L., G. R. Olivo, M. Chouteau, S. Perrouty, P. Shamsipour, R. Enkin, W. A. Morris, L. Feltrin, and R. Thiémonge, 2018, Predicting rock type and detecting hydrothermal alteration using machine learning and petrophysical properties of the Canadian Malartic ore and host rocks, Pontiac Subprovince, Québec, Canada: Ore Geology Reviews, **96**, 130–145, doi: 10.1016/j.oregeorev.2018.04.011.

Bierlein, F. P., and S. Maher, 2001, Orogenic disseminated gold in Phanerozoic fold belts — Examples from Victoria, Australia and elsewhere: Ore Geology Reviews, **18**, 113–148, doi: 10.1016/S0169-1368(01)00019-1.

Blacklock, N., 2015, Vein characterization using structural controls and petrographic analysis at Cartier zone in the Canadian Malartic property at Malartic, Quebec: B.Sc. thesis, Queen's University.

Derry, D. R., 1939, The geology of the Canadian Malartic gold mine, N. Quebec: Economic Geology, **34**, 495–523, doi: 10.2113/gsecongeo.34.5.495.

De Souza, S., B. Dubé, V. McNicoll, C. Dupuis, P. Mercier-Langevin, R. A. Creaser, and I. Kjarsgaard, 2016, Geology and hydrothermal alteration of the world-class Canadian Malartic gold deposit: Genesis of an Archean stockwork-disseminated gold deposit in the Abitibi greenstone belt: Reviews in Economic Geology, **19**, 263–291.

Dubé, B., and P. Gosselin, 2007, Greenstone-hosted quartz-carbonate vein deposits, *in* W. D. Goodfellow, ed., Mineral deposits of Canada: A synthesis of major deposit types, district metallogeny, the evolution of geological provinces, and exploration methods: Geological Association of Canada, Mineral Deposits Division, Special Publication 5, 49–73.

Ford, K., P. Keating, and M. D. Thomas, 2007, Overview of geophysical signatures associated with Canadian ore deposits, *in* W. D. Goodfellow, ed., Mineral deposits of Canada: A synthesis of major deposit types, district metallogeny, the evolution of geological provinces, and exploration methods: Geological Association of Canada, Mineral Deposits Division, Special Publication 5, 939–970.

Fraser, D. C., 1978, Resistivity mapping with an airborne multicoil electromagnetic system: Geophysics, **43**, 144–172, doi: 10.1190/1.1440817.

Gaillard, N., A. E. Williams-Jones, J. R. Clark, P. Lypaczewski, S. Salvi, S. Perrouty, N. Piette-Lauzière, C. Guilmette, and R. L. Linnen, 2018, Mica composition as a vector to gold mineralization: Deciphering hydrothermal and metamorphic effects in the Malartic District, Québec: Ore Geology Reviews, **95**, 789–820, doi: 10.1016/j.oregeorev.2018.02.009.

Gervais, D., C. Roy, A. Thibault, C. Pednault, and D. Doucet, 2014, Technical Report on the mineral resource and mineral reserve estimates for the Canadian Malartic Property: Canadian Malartic Mine.

Groves, D. I., M. Santosh, R. J. Goldfarb, and L. Zhang, 2018, Structural geometry of orogenic gold deposits: Implications for exploration of world-class and giant deposits: Geoscience Frontiers, **9**, 1163–1177, doi: 10.1016/j.gsf.2018.01.006.

Helt, K. M., A. E. Williams-Jones, J. R. Clark, B. A. Wing, and R. P. Wares, 2014, Constraints on the genesis of the Archean oxidized, intrusion-related Canadian Malartic gold deposit, Quebec, Canada: Economic Geology, **109**, 713–735, doi: 10.2113/econgeo.109.3.713.

Large, R. R., V. V. Maslennikov, F. Robert, L. V. Danyushevsky, and Z. Chang, 2007, Multistage sedimentary and metamorphic origin of pyrite and gold in the giant Sukhoi Log deposit, Lena gold province, Russia: Economic Geology, **102**, 1233–1267, doi: 10.2113/gsecongeo.102.7.1233.

Perrouty, S., N. Gaillard, N. Piette-Lauzière, R. Mir, M. Bardoux, G. R. Olivo, R. L. Linnen, C. L. Bérubé, P. Lypaczewski, C. Guilmette, and L. Feltrin, 2017, Structural setting for Canadian Malartic style of gold mineralization in the Pontiac subprovince, south of the Cadillac Larder Lake deformation zone, Québec, Canada: Ore Geology Reviews, **84**, 185–201, doi: 10.1016/j.oregeorev.2017.01.009.

Perrouty, S., M. W. Jessell, Y. Bourassa, J. Miller, D. Apau, L. Siebenaller, G. Velásquez, L. Baratoux, L. Aillères, D. Béziat, and S. Salvi, 2015, The Wassa deposit: A poly-deformed orogenic gold system in southwest Ghana — Implications for regional exploration: Journal of African Earth Sciences, **112**, 536–547, doi: 10.1016/j.jafrearsci.2015.03.003.

Sansfaçon, R., and C. Hubert, 1990, The Malartic Gold District, Abitibi greenstone belt, Québec: Geological setting, structure and timing of gold emplacement Barnat, east-Malartic, Canadian Malartic and Sladen Mines, *in* M. Rive, P. Verpealst, Y. Gagnon, J. M. Lulin, G. Riverin, and A. Simard, eds., The northwestern Quebec polymetallic belt: A summary of 60 years of mining exploration: Canadian Institute of Mining and Metallurgy 43, Special Volume, 221–235.

Smith, M. J., 1980, Comparison of induced polarisation measurements over the Elura orebody: Exploration Geophysics, **11**, 77–80, doi: 10.1071/EG9804077.

Taves, R., 2016, Glacial dispersion of indicator minerals and geochemical pathfinders from the Canadian Malartic gold deposit Val d'Or, Quebec: Testing legacy data and new indicators: B.Sc. thesis, University of Waterloo.

Tølbøll, R. J., and N. B. Christensen, 2007, Sensitivity functions of frequency-domain magnetic dipole-dipole systems: Geophysics, **72**, no. 2, F45–F56, doi: 10.1190/1.2409623.

UBC-Geophysical Inversion Facility, 2014, DCIP3D: A program library for forward modelling and inversion of DC resistivity and induced polarization data over 3D structures, version 5.0, Developed under the consortium research project Joint/Cooperative Inversion of Geophysical and Geological Data: Department of Earth and Ocean Sciences, University of British Columbia, https://gif.eos.ubc.ca/software/dcip3d.

Veillette, J. J., 2004, Géologie des formations en surface et histoire glaciaire, Cadillac, Québec: Geological Survey of Canada, "A" Series Map 2019A, accessed on 6 October 2017, doi: 10.4095/215047.